

SAND2001-8011

Moody, N. R., Yang, N., Adams, D. P., Cordill, M. J., Bahr, D. F., (2002) Film thickness effects on interfacial fracture of epoxy bonds, In: *Polymer Interfaces and Thin Films* (edited by Karim, A., Frank, C. W., Russell, T. P., Nealy, P. F.) Materials Research Society, Pittsburgh, PA, **710**, DD10.6.1-DD10.6.6.

Film Thickness Effects on Interfacial Fracture of Epoxy Bonds

N. R. Moody, D. F. Bahr^{*}, M. S. Kent^{**}, J. A. Emerson^{**}, E. D. Reedy, Jr.^{**}

Sandia National Laboratories, Livermore CA 94550

^{*}Washington State University, Pullman, WA 99164

^{**}Sandia National Laboratories, Albuquerque, NM 87185

ABSTRACT

Nanoindentation test techniques were combined with deposition of highly stressed overlayers to study the interfacial fracture susceptibility of spin coated Epon 828/T403 on aluminized glass substrates as a function of film thickness. The test techniques required to induce fracture differed between samples. Nevertheless, the resulting interfacial fracture energies decreased monotonically with film thickness to a value near 0.5 J/m^2 . This value is higher than the 'true work of adhesion' for uncured epoxy oligomers on a methyl-terminated aluminum surface. However, it may indicate that we have irreversible specific interactions such as hydrogen bonding. Then 0.5 J/m^2 may be near the fundamental value for such an interaction, or the 'practical work of adhesion'.

INTRODUCTION

Adhesion is an important factor in controlling the reliability of thin polymer films on metal substrates. It is a critical factor as the need for small devices drives reductions in bond thickness to sub-micron size. However, our understanding of failure in these systems is limited by a lack of established test techniques for very thin layer systems. Traditional test techniques such as double cantilever beam sandwich samples [1] often require relatively thick films while peel tests are dominated by plastic energy contributions as the film is bent. [2] In addition, it is difficult to maintain uniform film thickness in traditional sandwich geometries when bonds are less than one micron thick. The work of Bagchi et al. [3,4], and more recently the work by Kriese and coworkers [5,6] and Zhuk et al [7] shows that these limitations can be overcome for testing thin metal and polymer films by deposition of a relatively hard highly stressed overlayer. In this study, we combined stressed overlayers with nanoindentation to study the effect of film thickness on the interfacial fracture of thin Epon 828/T403 films on aluminum. This system was chosen for study as the mechanical properties and structure are well characterized. [1] In addition, the interfacial fracture energy of 19 J/m^2 for 500 nm thick films on aluminum indicates relatively good adhesion.

MATERIALS AND PROCEDURE

The thin film test samples for this study were created by sputter depositing 200 nm of aluminum onto microscope glass slides to create the sample substrates. These substrates were plasma-cleaned and spin-coated with Epon 828/T403 in a resin to crosslinker ratio of 100:46 to thicknesses of 24 , 164 , 615 , and 11800 nm . The films were then given a $50^\circ\text{C}/24\text{h}+40^\circ\text{C}/24\text{h}$ cure.

The elastic modulus and hardness values of the films were measured using the continuous stiffness measurement option on a Nano Indenter IITM with a Berkovich diamond indenter at a superimposed excitation frequency of 45 Hz and displacement of 3 nm . An approach rate of 2 nm/s was used to minimize kinetic effects and surface contact was defined by the point of deviation in the phase angle versus displacement curve. All tests were conducted in air at 22°C , well below the glass transition temperature of 68°C .

Nanoindentation was used to induce fracture in the 11.8 nm thick film using an 8.3 nm radius conical diamond tip. Additional stress from tungsten overlayers was required for testing

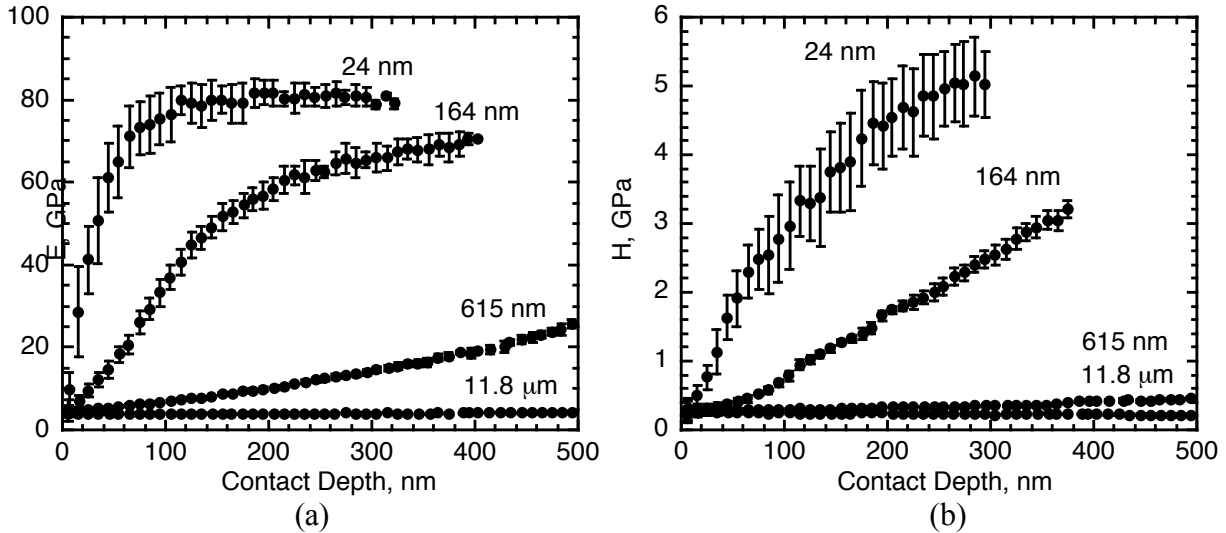


Figure 1. Nanoindentation gives an (a) average near surface elastic modulus of 4.35 GPa and (b) an average hardness of 250 MPa for all films. The error bars correspond to one standard deviation.

thinner films. Tungsten overlayer deposition was accomplished by placing the epoxy films into a sputter deposition chamber, evacuating to 3×10^{-6} torr, backfilling with 2.5 mtorr argon gas, and sputter depositing tungsten at a rate of 0.2 nm/s to a final thickness of 220 nm. A companion silica wafer showed that deposition induced a compressive residual stress in the tungsten films of 2.2 GPa. Following deposition, indentation fracture tests were conducted using the Nano Indenter IITM with a 1 μm radius conical diamond tip. All indentations were examined optically and several were examined using Atomic Force Microscopy.

RESULTS AND DISCUSSION

Mechanical Properties

Elastic modulus and hardness were obtained as a function of depth for each film as shown in Figure 1. In all films, the data reached a plateau near the surface giving an average near surface modulus of 4.35 GPa. The corresponding hardness values for all films averaged 250 MPa. From these values, a yield strength of 115 MPa was estimated for all films following the empirical relationship between hardness and yield strength of glasses and glassy polymers observed by Marsh. [8] These values are slightly higher than bulk sample modulus of 3.5 GPa and yield strength of 90 MPa measured using compression tests. [1]

Fracture

Deposition of the tungsten overlayers on companion samples triggered extensive interface delamination and telephone cord blistering that completely covered the 24 nm thick film. (Figure 2a) There was also some telephone cord blistering on the 164 nm thick film. Nanoindentation was then used to induce interfacial fracture in the 164 nm, 615 nm, and 11.8 μm films where telephone cord blistering did not occur. Tests on the 164 nm thick film triggered telephone cord blistering whereas tests on the 615 nm thick epoxy film system triggered formation of large circular blisters. (Figure 2b) [9] Close examination of the indentations and accompanying blisters using Atomic Force Microscopy showed that material was not compressed into the tungsten

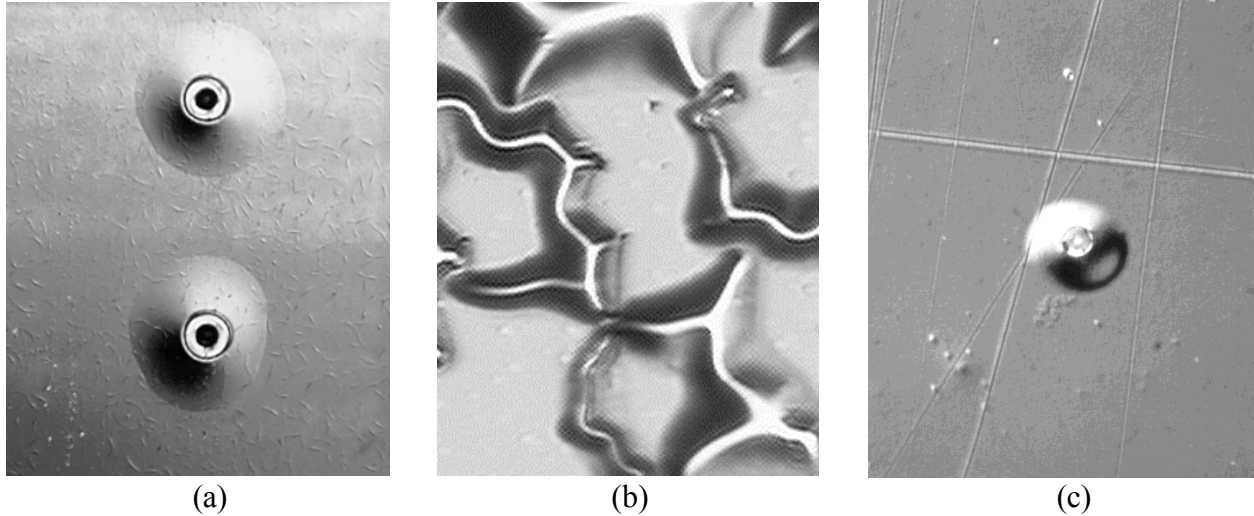


Figure 2. The 11.8 mm thick film (a) delaminated during nanoindentation. Stressed overlayers triggered telephone cord blistering in the (b) 24 nm thick film. Nanoindentation triggered (c) circular blister formation in 164 nm thick films with stressed overlayers.

overlay. The overlayer wrapped around the indenter, increasing the effective indentation size. This strongly suggests that indentation served to nucleate fracture, but once fracture nucleated, delamination and blister formation were driven by the residual stresses in the overlayer. [9] Tests on the 11.8 mm thick epoxy film also triggered large film delaminations. However, the stresses triggering delamination were not sufficient to drive blister formation. (Figure 2c) The conical shape to the delaminated regions is most likely due to adhesion of the film to the diamond indenter as the indenter is withdrawn from the sample at the end of each test.

We were unable to determine whether epoxy remained on the substrate surface as previously observed for films on glass [10-12] or whether failure occurred along the film-substrate interface as observed for this film system on aluminum. [1] However, we used a peel test to remove some films from the aluminized substrates and then examined the substrates using optical microscopy with Nemarski contrast and Attenuated Total Reflectance Spectroscopy. No epoxy was observed on the substrates suggesting that failure occurred interfacially.

Fracture Energy Analysis

The telephone cord and circular blisters provide the data from which interfacial fracture energies were obtained using solutions for film systems where residual stresses drive fracture. These solutions were originally derived for single layer film-on-substrate systems [13-15]. Work by Bagchi et al. [3,4] and more recently by Kriese et al. [5,6] extended these solutions to multilayer systems by treating the multilayer film as a single film of the same total thickness with a transformed moment of inertia. Account was also taken for the differences in elastic constants, thickness, and residual stress of each layer and their contribution to the total strain energy of the system. Blister growth occurs along the circular front while the width of the telephone cord blister remains fixed giving a fracture energy along the side wall of,

$$\Gamma(\sigma) = \frac{\sigma^2 h^2}{2E} (\sigma_r + 3\sigma_b) \quad (1)$$

The fracture energy for the circular blisters under small scale buckling conditions is given by,

$$G(\sigma) = \frac{2\sigma_f^2 h^2 \sigma_r^2}{E[1 + 0.9021(1 - \nu_f)]} \left(\frac{\sigma_b}{\sigma_r} \right)^2 \quad (2)$$

In these expressions, E is the bilayer elastic modulus, ν is the bilayer Poisson's ratio, h, is the tungsten and epoxy film thickness, σ_r , is the effective residual stress, and σ_b , is the effective bilayer delamination stress.

The fracture energies for the 11.8 μm thick film delaminations were estimated [16] following the analyses of Thouless [17], Ritter et al. [18], and Rosenfeld et al. [19] In these analyses, delamination is assumed to initiate from an internal discontinuity of radius a, the contact radius. The delaminated region is modeled as an elastic disc under plane stress, incorporating only radial and circumferential stresses. Integrating the normal stress and strains over the delaminated region volume gives the following strain energy release rate for fracture, [17-19]

$$G(\sigma) = \frac{2\sigma_f^2 h^2 \sigma_o^2}{E\nu_f + \nu_f + (b/a)^2(1 - \nu_f)} \quad (3)$$

where ν_f and E_f are Poisson's ratio and modulus of the film respectively, h is the film thickness, b is the delamination radius, and σ_o is the uniform radial stress on the edge of the contact zone. Assuming that hardness, H, is constant through the film thickness, σ_o is set equal to $(H - \sigma_{ys})$.

The measured fracture energies are mixed mode values, comprised of mode I normal and mode II shear loading. Interfacial fracture is often treated as a mode I failure with mode I energies at crack arrest set equal to the practical work of adhesion [13]. The relationship between mode I and mode II contributions is not well defined. However, several criteria have been proposed to characterize interfacial fracture energy based on the phase angle of loading, ψ , defined as the tangent of the ratio between shear and normal forces at the crack tip. Of these criteria, the following is often found to realistically reproduce data for interfacial fracture [13],

$$G_I = G(\psi) / \left\{ 1 + \tan^2[(1 - \nu)\psi] \right\} \quad (4)$$

where ν is a material parameter equal to 0.3 for most materials and ψ is the phase angle of loading. It should be noted that significant reservations have been raised concerning determination of the phase angle for multilayer systems [5]. Nevertheless, a phase angle of loading can be estimated using solutions for circular blister formation by Hutchinson and Suo [13],

$$\psi = \tan^{-1} \left[\frac{h\Delta N}{\sqrt{12M}} \cos \theta + \frac{h\Delta N}{\sqrt{12M}} \sin \theta \right] \quad (5)$$

where ΔN is the in-plane stress, M is the bending moment, and θ is a dimensionless function describing the elastic mismatch between the film and the substrate. The value for $h\Delta N/(\sqrt{12M})$ is determined from numerical solutions based on an effective loading parameter, σ_r/σ_b . [13] Accounting for the effect of elastic mismatch between the epoxy and aluminum, ν is set equal to

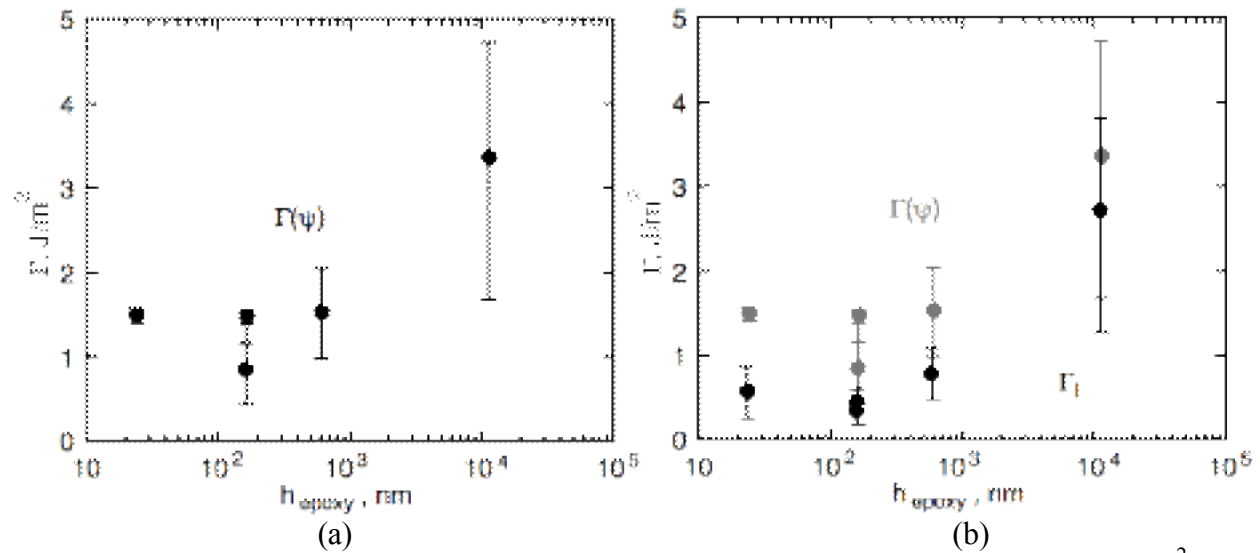


Figure 3. Fracture energies decrease with decreasing film thickness to (a) a value of 1.6 J/m² for the 24 nm thick film. These are mixed mode values comprised of mode I normal and mode II shear contributions. The (b) mode I contributions decrease to 0.5 J/m². The error bars denote the full range of measured values for each sample.

-53.1°. [16] The phase angle of loading for the delamination fracture of the 11.8 μm thick films is approximately equal to 0°. [13,16,20]

The results are given in Figure 3 and show that measured fracture energies decrease with decreasing film thickness to a value of 1.6 J/m² for the 24 nm thick film. The corresponding mode I values decrease to 0.5 J/m². This is significantly higher than the work of adhesion for uncured epoxy oligomers on a methyl-terminated aluminum surface of 50 mJ/m². [1] However, this value does not account for chemical interactions that may form upon cure. The value near 0.5 J/m² may indicate that we have irreversible specific interactions such as hydrogen-bonding. If irreversible interactions form upon curing, the ‘true work of adhesion’ is undefined. Then 0.5 J/m² may be near the fundamental value for such an interaction, or the ‘practical work of adhesion’.

SUMMARY

In this study we combined nanoindentation with stressed overlayers to determine the effect of film thickness on the interfacial fracture energy of Epon 828/T403. The films were spin coated onto aluminized substrates to four thicknesses ranging from 24 nm to 11.8 μm. Nanoindentation gave a near surface elastic modulus of 4.35 GPa and a hardness equal to 250 MPa with a film strength of 115 MPa. The combination of nanoindentation and deposition of a highly stressed tungsten overlayer were used to induce delamination and blister formation in the films. Interfacial fracture energies were then determined using mechanics-based models modified for multilayer films. Interestingly, the results parallel thin metal film behavior where interfacial fracture energies decreased to 1.6 J/m² and mode I components to 0.5 J/m² as film thickness decreased to 24 nm. This value is significantly higher than the work of adhesion for uncured epoxy oligomers on a methyl-terminated aluminum surface. Nevertheless, it may indicate that we have irreversible specific interactions such as hydrogen bonding. Then 0.5 J/m² may be near the fundamental value for such an interaction, or the ‘practical work of adhesion’.

ACKNOWLEDGMENTS

The authors wish to thank Christy Woodcock and Kirsten Schafer from Washington State University for their technical assistance and Yvete Toivola from the University of Minnesota for performing ATR spectroscopy. The authors also gratefully acknowledge the support of U.S. DOE Contract DE-AC04-94AL85000.

REFERENCES

1. M. S. Kent, E. D. Reedy, and M. J. Stevens, Molecular-to-Continuum Fracture Analysis of Thermosetting Polymer/Solid Interfaces, Sandia Report SAND2000-0026 (2000).
2. Wei and J. W. Hutchinson, *Int'l. Journal of Fracture*, **9**, 315 (1998).
3. A. Bagchi and A. G. Evans, *Thin Solid Films*, **286**, 203 (1996).
4. A. Bagchi, G. E. Lucas, Z. Suo, and A. G. Evans, *J. Mater. Res.*, **9**, 1734 (1994).
5. M. D. Kriese, W. W. Gerberich, and N. R. Moody, *J. Mater. Res.*, **14**, 3007 (1999).
6. M. D. Kriese, N. R. Moody, and W. W. Gerberich, *Acta mater.*, **46**, 6623 (1998).
7. A. V. Zhuk, A. G. Evans, J. W. Hutchinson, and G. M. Whitesides, *J. Mater. Res.*, **13**, 3555 (1998).
8. D. M. Marsh, *Proc. Roy. Soc. A*, **279**, 420 (1963).
9. N. R. Moody, D. F. Bahr, M. S. Kent, J. A. Emerson, E. D. Reedy, Jr., in *Fundamentals of Nanoindentation and Nanotribology II*, edited by R. F. Cook, S. P. Baker, S.G. Corcoran, and N. R. Moody, (Mater. Res. Soc. Proc., **649**, Pittsburgh, PA, 2001) pp. Q6.3.1-6.
10. J. G. Swadener, K. M. Liechti, and A. L. de Lozanne, *J. Mech. Phys. Solids*, **47**, 223 (1999).
11. R. K. Agrawal and L. T. Drzal, *J. Adhesion*, **54**, (1995) p. 79-102.
12. R. K. Agrawal and L. T. Drzal, *J. Adhesion Sci. Tech.*, **9**, 1381 (1995).
13. J. W. Hutchinson and Z. Suo, in *Advances in Applied Mechanics*, edited by J. W. Hutchinson and T. Y. Wu (Academic Press Inc., vol. **29**, New York 1992) pp. 63-191.
14. D. B. Marshall and A. G. Evans, *J. Appl. Phys.*, **56**, 2632 (1984).
15. A. G. Evans and J. W. Hutchinson, *Int. J. Solids Struct.*, **20**, 455 (1984).
16. A. Strojny, N. R. Moody, J. A. Emerson, W. W. in *Polymer Systems*, S. H. Anastasiadis, A. Karim, G. S. Ferguson, eds., (Mater. Res. Soc. Proc, **629**, Pittsburgh, PA, 2000) p. F5.13.1-6.
17. M. D. Thouless, *Acta Metall.*, **36**, 3131 (1988).
18. J. E. Ritter, T. J. Lardner, L. Rosenfeld, and M. R. Lin, *J. Appl. Phys.*, **66**, 3626 (1989).
19. L. G. Rosenfeld, J. E. Ritter, T. J. Lardner, and M. R. Lin, *J. Appl. Phys.*, **67**, 3291 (1990).
20. Z. Suo and J. W. Hutchinson, *Mater. Sci. Engng.*, **A107**, 135 (1989).